1522 | Tractive performance of rigid wheel in granular media using coarse-scale DEM models

Bohumir Jelinek [a]*, Angela Card [a], George L. Mason [a], Thomas James [a], Karl Grebner [a], Thomas Skorupa [b], Jody D. Priddy [c]

[a] *Center for Advanced Vehicular Systems, Mississippi State University, Mississippi State, Mississippi, United States*

[b] *U.S. Army Combat Capabilities Development Command Ground Vehicle Systems Center, Warren, Michigan, United States*

[c] *U.S. Army Engineer Research and Development Center, Geotechnical and Structures Laboratory, Vicksburg, Mississippi, United States*

** Corresponding author: bj48@cavs.msstate.edu*

ABSTRACT

Understanding the interaction between wheel and granular media in variable loading conditions is critical for prediction of net traction of wheeled and tracked vehicles in off-road environments. The discrete element method (DEM) is routinely used for modeling vehicle performance, but although simulations seem realistic, the method's accuracy is often not fully established.

In this work, the DEM modeling accuracy is assessed by the comparison of ten DEM soil models with laboratory soil-bin measurements of the net traction, gross traction, and sinkage of a wheel operating in sand. Laboratory soil-bin measurements, serving as a reference for DEM simulations, were taken from physical experiments (Shinone et al., 2010) examining a 165/60R13 wheel with constant circumferential velocity of 97.6 mm/s and vertical contact load of 980 N operating in powered conditions under slips in the range of -5.9% to 54.8%. The set of ten DEM models representing particle-particle and particle-geometry interactions was a subset of the Generic EDEM Material Model (GEMM) database from Altair®'s EDEM™ software package, choosing the best match to the bulk density and angle of repose for dry sand. Parameters for particle-wheel interactions were left identical to GEMM parameters for particle-geometry interactions.

Given the large particle size and no additional calibration of the DEM model, identifying a single GEMM material model with reasonable similarity for the net traction and sinkage is encouraging. The largest discrepancy between DEM and the lab experiment was observed at negative slips. A need for smaller particle size and further calibration are suggested for a future effort.

Keywords
Discrete element method
Net traction
Gross traction
Sinkage
Slip

1. Introduction

Prediction of vehicle mobility for vehicles in off-road environment presents a challenge for agriculture, construction, military, and space exploration. Suspension and powertrain systems are usually characterized well, but the accuracy of mobility models suffers from hard-to-predict terrain response. The subgrade materials that a vehicle operates on may include rock, gravel, sand, silt, clay soil, or their mixtures with various degrees of saturation. Even relatively homogeneous subgrade is hard to model numerically at the continuum level due to large deformation and material non-linearity, as well as at the particle level due to the complex geometry of soil particles, variability in contact mechanics, and high number of degrees of freedom involved. Predictions of mobility using numerical models must therefore compromise between sufficiently detailed representation and capabilities of high-performance computing.

Multiple studies have used DEM to characterize the interaction of granular subgrades with rigid and flexible wheels. The bulk of DEM work has focused on predicting the mobility of rovers on Earth, the Moon, and Mars in regolith sediments (Nakashima et al. 2010; Knuth et al. 2012; Nakashima and Kobayashi, 2014; Johnson et al., 2015, 2017) exploring the effects of gravity on sinkage and motion resistance of a rigid rover wheel. Tractive and steering performance of off-road wheels on dry sand was analyzed by Du et al. 2017a, 2017b, 2018. These studies examined the effects of lug type, intersection of lug bars, and central angle, with the objective to improve performance prediction for straight and steered performance. The scope of off-road mobility modeling was extended beyond rigid wheels by introducing finite element pneumatic tire model (Recuero et al., 2017). Vertical stress under the wheels of agricultural machinery obtained from DEM using Yade (Šmilauer et al., 2015) was compared with pseudo-analytical continuum model and field measurements field measurements (De Pue et al., 2020, 2019; De Pue and Cornelis, 2019).

Yang et al., (2020) performed DEM-FEM (Finite Element Method) simulations of flexible multi-layer tire on gravel at 10%, 20%, and 30% slip and showed a reasonable agreement of sinkage, gross tractive effort, and tractive force with experiment. These models, however, require a careful calibration (Coetzee, 2017; Zeng et al., 2020a, 2020b), and, in many cases, non-spherical particles are used to better match the experiments (Coetzee, 2020).

In this work, a laboratory experiment to predict tractive performance of a wheel in sand conducted by Shinone et al., 2010 is compared with numerical simulations deploying ten different out-of-the-box coarse-grain DEM models selected to mimic sand-like macroscopic properties. The goal of the study is to evaluate capability of coarse-grain DEM models to predict the net traction, gross traction, and sinkage of a smooth wheel operating in sand under braked and powered conditions.

2. DEM methodology

A particle bed to simulate wheel-soil interactions was generated using particle-factory functionality of the Altair®'s EDEM™ software. The particle bed was assembled from five identical material blocks repeated along the longitudinal direction. Only the particles in a single block were settled under periodic boundary conditions to lower the simulation time needed to populate the bed with particles. A smooth-surface cylindrical wheel without tread was constructed from triangular facets. Figure 1 illustrates the wheel and enclosing box while Table 1

https://doi.org/10.56884/ABCD1234 *(ed. note: ISTVS will update your paper's DOI)*
ISBN 978-1-942112-55-6

specifies their dimensions. Figure 1 illustrates the wheel and enclosing box while Table 1 specifies their dimensions.

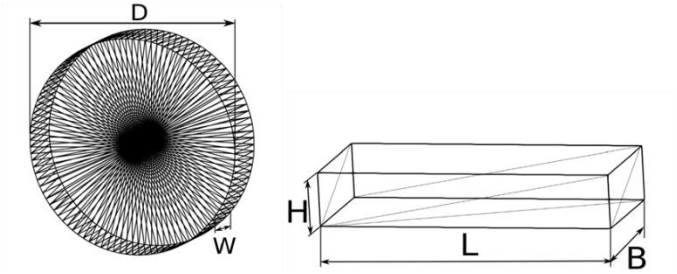

Fig. 1. Triangular facet representation of the wheel and enclosing box

Table 1
Wheel and Box Dimensions

Property	Symbol	Units	Value
Wheel diameter	D	cm	53.49
Wheel width	W	cm	16.99
Wheel weight	F_G	N	980.33
Box length	L	cm	301.5
Box width	B	cm	48.0
Box depth	H	cm	60.5
Soil depth	h	cm	60
Number of particles	N	-	97152

Ten different DEM soil models with sand-like macroscopic response were evaluated. Models were chosen from Altair®'s EDEM™ GEMM database based on the following requirements: a bulk density range of 1500-2000 kg/m^3 and an angle of repose of 34 degrees. To represent homogeneous soil with a degree of randomness, particle sizes were scaled to produce a normal distribution. Blocks were duplicated within particle beds and then settled to negligible kinetic energies. To control particle bed variation between simulations, only particle properties were adjusted with Altair's EDEM.PY Python package. Table 2 and Table 3 present GEMM particle properties.

Table 2
Particle Properties

Mat. #	1507	1301	1311	1615	1706
ν	0.25	0.25	0.25	0.25	0.25
ρ	3300	3300	3300	3300	3300
E	10	10	10	10	10
e^p	0.35	0.15	0.55	0.55	0.35
$\mu_s{}^p$	0.92	0.68	0.68	1.04	1.16
$\mu_r{}^p$	0	0	0	0	0
γ^p	4.5	0	0	18	0
e^g	0.5	0.5	0.5	0.5	0.5
$\mu_s{}^g$	0.45	0.45	0.45	0.45	0.45
$\mu_r{}^g$	0.15	0.15	0.15	0.15	0.15
γ^g	4.5	0	0	18	0

Table 3
Particle Properties

Mat. #	1111	1501	1308	1105	1636
ν	0.25	0.25	0.25	0.25	0.25
ρ	3300	3300	3300	3300	3300
G	10	10	10	10	10
e^p	0.55	0.35	0.35	0.15	0.75
$\mu_s{}^p$	0.44	0.92	0.68	0.44	1.04
$\mu_r{}^p$	0	0	0	0	0.05
γ^p	0	18	9	18	0
e^g	0.5	0.5	0.5	0.5	0.5
$\mu_s{}^g$	0.45	0.45	0.45	0.45	0.45
$\mu_r{}^g$	0.15	0.15	0.15	0.15	0.15
γ^g	0	18	9	18	0

*a superscript of *p* implies particle-particle interaction while *g* is a particle-geometry interaction

All particles were a multi-spherical shape. Individual spheres had a radius of 9.5mm with a fixed overlap. Figure 2 visualizes the multi-sphere particles.

Fig. 2. Multi-spherical particle shape

The Hertz-Mindlin (no slip) and Hertz-Mindlin with JKR models were used to represent DEM contact models. Hertz-Mindlin (Mindlin and Deresiewicz, 1953) is the default model used in EDEM due to its accurate and efficient force calculation (1993). The Hertz-Mindlin JKR model was used for particles with a non-zero JKR coefficient. For Hertz-Mindlin, the normal force is a function of normal overlap δ_n:

$$F_x = \frac{4}{3} E^* \sqrt{R^*} \delta_n^{\frac{3}{2}} \tag{1}$$

where the E^* is the equivalent Young's Modulus and R^* is the equivalent radius. They are defined as:

$$\frac{1}{R^*} = \frac{1}{R_i} + \frac{1}{R_j} \tag{2}$$

$$\frac{1}{E^*} = \frac{(1-v_i^2)}{E_i} + \frac{(1-v_j^2)}{E_j} \tag{3}$$

with E^i, v^i, R^i, and E^j, v^j, R^j being the Young's Modulus, Poisson ratio, and radius of each sphere in contact. Additionally, there is a damping force, $F_n{}^d$, given by:

$$\boldsymbol{F_n^d} = -2\sqrt{\frac{5}{6}}\beta\sqrt{S_n m^*}\,\boldsymbol{v_n^{rel}} \tag{4}$$

$$m^* = \left(\frac{1}{m_j} + \frac{1}{m_i}\right)^{-1} \quad (5)$$

$$\beta = \frac{-\ln e}{\sqrt{ln^2 e + \pi^2}} \quad (6)$$

$$S_n = 2E^*\sqrt{R^*\delta_n} \quad (7)$$

where m* is the equivalent mass, $\boldsymbol{v_n^{rel}}$ is the normal component of the relative velocity, β, and S_n (the normal stiffness). The constant e is the coefficient of restitution, the tangential force, F_t, depends on the tangential overlap δ_t and the tangential stiffness S_t.

$$F_t = -S_t\delta_t \quad (8)$$

$$S_t = 8G^*\sqrt{R^*\delta_n} \quad (9)$$

Here, G^* is the equivalent shear modulus. Additionally, tangential damping is defined as:

$$\boldsymbol{F_t^d} = -2\sqrt{\frac{5}{6}}\beta\sqrt{S_t m^*}\boldsymbol{v_t^{rel}} \quad (10)$$

where $\boldsymbol{v_t^{rel}}$ is the relative tangential velocity. The tangential force is limited by Coulomb friction, $\mu_s F_n$, where μ_s is the coefficient of static friction.

The Hertz-Mindlin contact model with JKR cohesion (Johnson et al., 1971) allows modelling of cohesive materials. It calculates the normal force as a function of overlap δ_n and the surface energy parameter γ as follows:

$$F_{JKR} = -4\sqrt{\pi\gamma E^*}a^{3/2} + \frac{4E^*}{3R^*}a^3, \quad (11)$$

$$\delta_n = \frac{a^2}{R^*} - \sqrt{\frac{4\pi\gamma a}{E^*}} \quad (12)$$

where E^* is the equivalent Young modulus and R^* is the equivalent radius from Eq. (2). Wheel slip and circumferential velocity were used as an initial condition to each system. Wheel slip is defined as:

$$i = 1 - \frac{v_f}{\omega r} \quad (13)$$

Equation 13 defines i as wheel slip, v_f as the wheel forward velocity, ω as wheel angular displacement, and r as wheel radius. Post-processing values such as net traction and gross traction were calculated using Eq. 13 and Eq. 14, respectively. Sinkage amount was based on the initial position of the suspended wheel.

$$F^x = \sum_j F_j^x \quad (14)$$

$$T = \sum_j F_j^t d_j \quad (15)$$

F^x is the forward component of the contact force, F^t is the wheel-surface-tangential component of the contact force, D is the wheel diameter and d_j is distance from the contact point to the wheel axis. F^t has negative/positive sign if the force acts to increase/decrease wheel rotation.

3. Results

With a load of 980 N, the wheel was placed -1.3 meters away from the center of the bed. By coupling a driving program to EDEM, the wheel moved at a constant circumferential velocity of 97.6 millimeters per second to the final position of 1.3 meters. With one degree of freedom, the wheel only moved freely along the surface's normal axis (allowing sinkage). Figure 3 shows the initial position of the system.

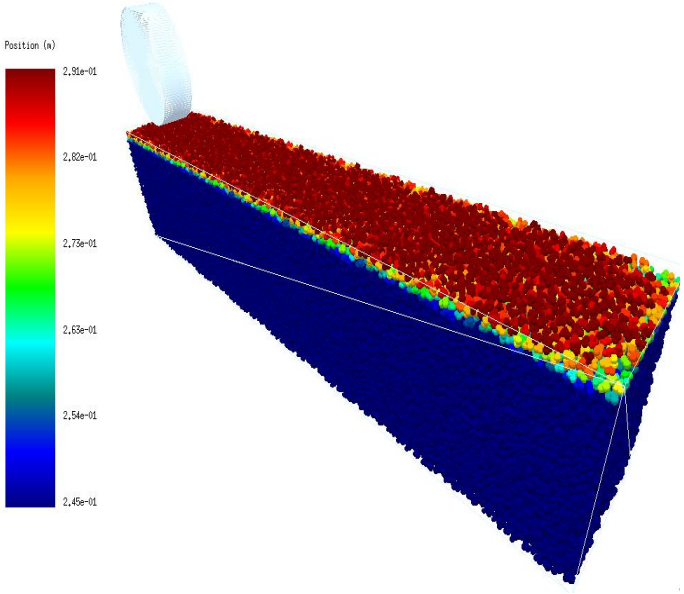

Fig. 3. Initial position: GEMM 1636, 45.8% slippage

Figure 4 shows a final state of a system with sinkage.

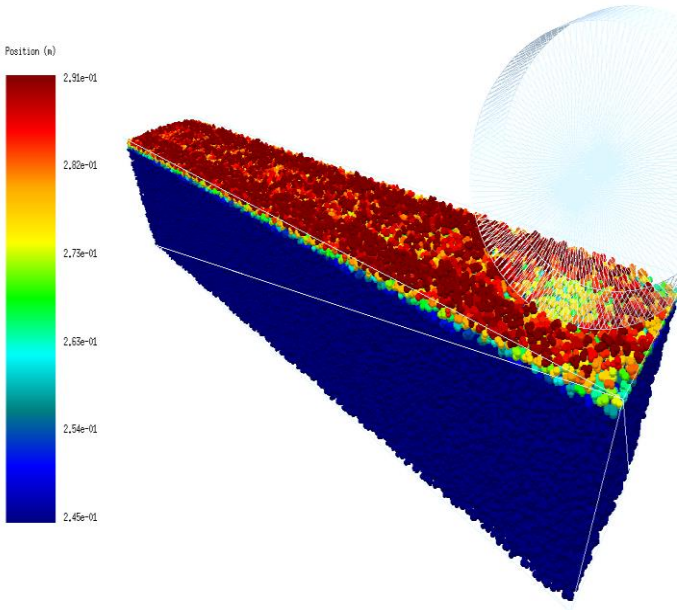

Fig. 4. Final position: GEMM 1636, 45.8% slippage

For each particle, wheel slippage ranged from -5.9% to 54.8%. Net traction, gross traction, and wheel height were plotted at each time step. Figures 5, 6, and 7 show plots of these values, for GEMM 1636 at 45.8% wheel slippage, over the simulation span. Initial data outliers are due to the wheel dropping above the surface.

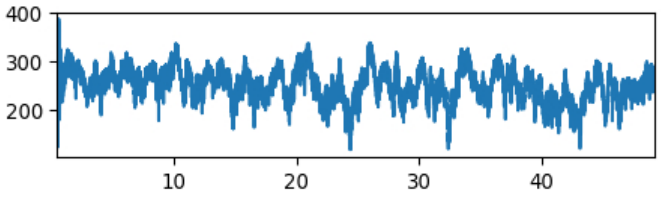

Fig. 5. Net traction (N) v. time (s): GEMM 1636, 45.8% slippage

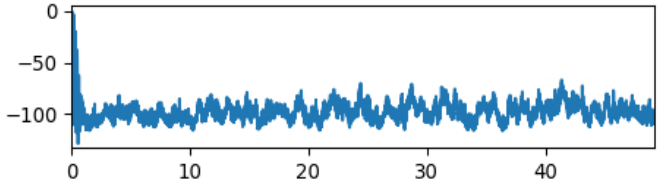

Fig. 6. Gross traction (Nm) v. time (s): GEMM 1636, 45.8% slippage

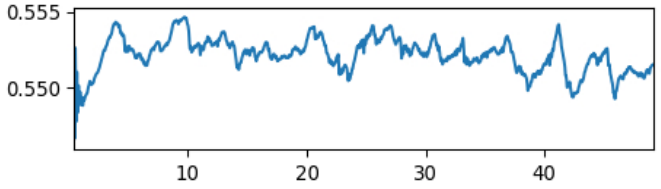

Fig. 7. Center of mass height (m) v. time (s): GEMM 1636, 45.8% slippage

Figures 8 and 9 show average net and gross traction. Data outside the interval of -1 meter to 1 meter was excluded.

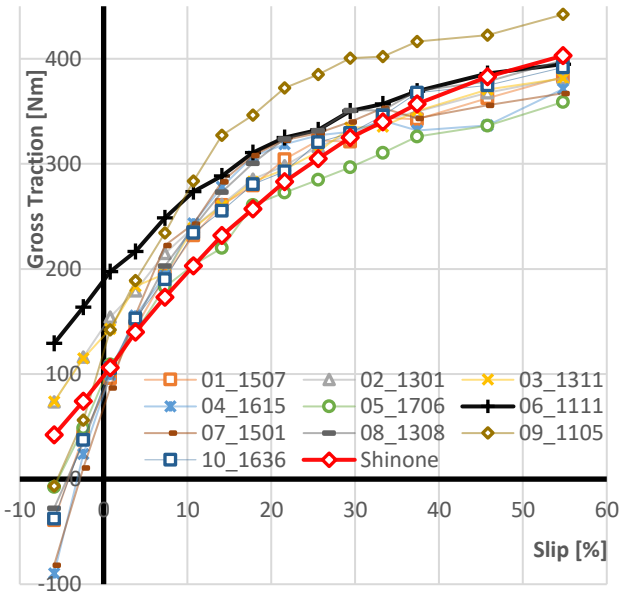

Fig. 8. Gross tractive effort

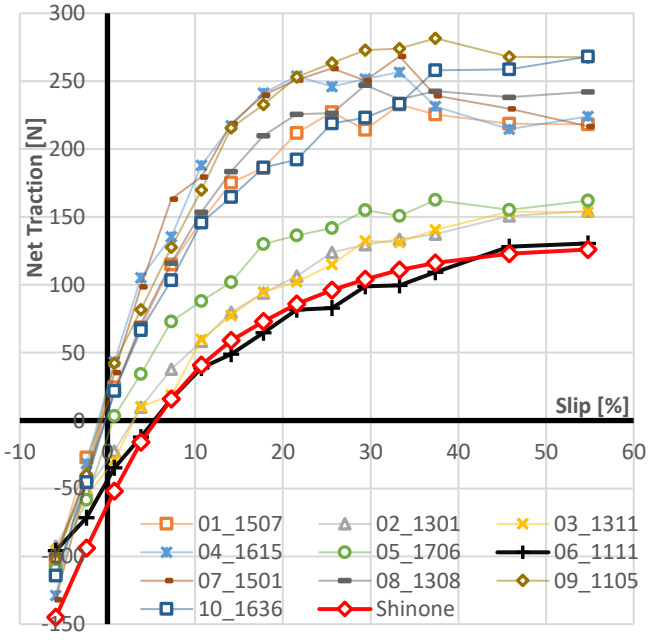

Fig. 9. Net tractive effort (drawbar pull)

Figure 10 shows wheel sinkage based on the lowest point of the wheel contact surface and the uncompressed height of the particle bed.

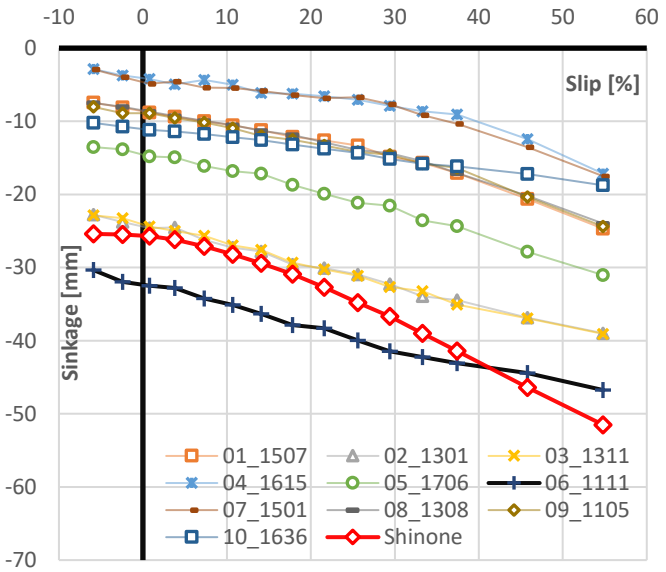

Fig. 10. Sinkage

4. Conclusions and future work

Out of ten materials selected from Altair®'s EDEM™ Generic Material Model (GEMM) database to match macroscopic properties of dry sand, GEMM material number 1111 provided the best agreement with lab test results reported by Shinone et al., 2010. The simulation results are similar to the experiment. Net traction was the most accurate model except that slightly lower values occurred at negative slips. Sinkage was overestimated by up to 25% for slips lower than 40% and underestimated by up to 10% for slips higher than 40%. The gross traction agrees well with DEM results for a slip larger than 40%, while at lower positive and negative slips the gross traction is overestimated by up to 200% at the slip of -5.9%.

5. Nomenclature

a	Contact radius	[m]
B	Box width	[m]
D	Wheel diameter	[m]
d_j	distance from the j-th particle wheel contact point to the wheel axis	[m]
e	Coefficient of restitution	[]
E	Young's modulus	[m]
F^d	Damping force	[m]
F_G	Wheel weight	[N]
F_r	Rolling friction force	[N]
F_s	Static friction force	[N]
F_x	Forward component of force on wheel	[N]
G	Shear modulus	[MPa]
H	Box depth	[m]
h	Soil depth	[m]
i	Wheel slip	[]
L	Box length	[m]
m	mass	[kg]
N	Number of particles	[]
R	Hertz-Mindlin radius	[m]
S	Stiffness	[N/m]
T	Gross tractive effort	[Nm]
v_f	Forward component of wheel velocity	[m/s]
v_t^{rel}	Relative tangential velocity	[m/s]
W	Wheel width	[m]
α	Contact overlap	[m]
β	Relative velocity	[m/s]
γ	JKR surface energy parameter	[J/m²]
δ	Overlap	[m]
μ	Coefficient of friction	[]
ν	Poisson's ratio	[]
ρ	Bulk Density	[kg/m³]
ω	Angular displacement	[1/s]

6. Acknowledgements

This material is based upon research conducted under contract W912HZ-22-C0004 with the U.S. Army Engineer Research and Development Center (ERDC). The views and conclusions contained herein are those of the authors and should not be interpreted as necessarily representing the official policies or endorsements, either expressed or implied, of ERDC or the U.S. Government.

7. Declaration of competing interest

The authors declare that they have no known competing financial interests or personal relationships that could have appeared to influence the work reported in this paper.

8. References

Coetzee, C., 2020. Calibration of the discrete element method: Strategies for spherical and non-spherical particles. Powder Technol. 364, 851–878.

Coetzee, C.J., 2017. Review: Calibration of the discrete element method. Powder Technol. 310, 104–142.

De Pue, J., Cornelis, W.M., 2019. DEM simulation of stress transmission under agricultural traffic Part 1: Comparison with continuum model and parametric study. Soil Tillage Res. 195, 104408.

De Pue, J., Di Emidio, G., Verastegui Flores, R.D., Bezuijen, A., Cornelis, W.M., 2019. Calibration of DEM material parameters to simulate stress-strain behaviour of unsaturated soils during uniaxial compression. Soil Tillage Res. 194, 104303.

De Pue, J., Lamandé, M., Schjønning, P., Cornelis, W.M., 2020. DEM simulation of stress transmission under agricultural traffic Part 3: Evaluation with field experiment. Soil Tillage Res. 200, 104606.

Du, Y., Gao, J., Jiang, L., Zhang, Y., 2018. Development and numerical validation of an improved prediction model for wheel-soil interaction under multiple operating conditions. J. Terramechanics 79, 1–21.

Du, Y., Gao, J., Jiang, L., Zhang, Y., 2017a. Numerical analysis of lug effects on tractive performance of off-road wheel by DEM. J. Braz. Soc. Mech. Sci. Eng. 39, 1977–1987.

Du, Y., Gao, J., Jiang, L., Zhang, Y., 2017b. Numerical analysis on tractive performance of off-road wheel steering on sand using discrete element method. J. Terramechanics 71, 25–43.

Johnson, J.B., Duvoy, P.X., Kulchitsky, A.V., Creager, C., Moore, J., 2017. Analysis of Mars Exploration Rover wheel mobility processes and the limitations of classical terramechanics models using discrete element method simulations. J. Terramechanics 73, 61–71.

Johnson, J.B., Kulchitsky, A.V., Duvoy, P., Iagnemma, K., Senatore, C., Arvidson, R.E., Moore, J., 2015. Discrete element method simulations of Mars Exploration Rover wheel performance. J. Terramechanics 62, 31–40.

Johnson, K.L., Kendall, K., Roberts, A.D., 1971. Surface energy and the contact of elastic solids. Proc. R. Soc. Lond. Math. Phys. Sci. 324, 301–313.

Knuth, M.A., Johnson, J.B., Hopkins, M.A., Sullivan, R.J., Moore, J.M., 2012. Discrete element modeling of a Mars Exploration Rover wheel in granular material. J. Terramechanics 49, 27–36.

Mindlin, R.D., Deresiewicz, H., 1953. Elastic Spheres in Contact Under Varying Oblique Forces. J. Appl. Mech. 20, 327–344.

Nakashima, H., Fujii, H., Oida, A., Momozu, M., Kanamori, H., Aoki, S., Yokoyama, T., Shimizu, H., Miyasaka, J., Ohdoi, K., 2010. Discrete

element method analysis of single wheel performance for a small lunar rover on sloped terrain. J. Terramechanics 47, 307–321.
Nakashima, H., Kobayashi, T., 2014. Effects of gravity on rigid rover wheel sinkage and motion resistance assessed using two-dimensional discrete element method. J. Terramechanics 53, 37–45.
Recuero, A., Serban, R., Peterson, B., Sugiyama, H., Jayakumar, P., Negrut, D., 2017. A high-fidelity approach for vehicle mobility simulation: Nonlinear finite element tires operating on granular material. J. Terramechanics 72, 39–54.
Shinone, H., Nakashima, H., Takatsu, Y., Kasetani, T., Matsukawa, H., Shimizu, H., Miyasaka, J., Ohdoi, K., 2010. Experimental Analysis of Tread Pattern Effects on Tire Tractive Performance on Sand using an Indoor Traction Measurement System with Forced-slip Mechanism. Eng. Agric. Environ. Food 3, 61–66.
Šmilauer, V., others, 2015. Yade Documentation 2nd ed. The Yade Project.
Yang, P., Zang, M., Zeng, H., 2020. DEM–FEM simulation of tire–sand interaction based on improved contact model. Comput. Part. Mech. 7, 629–643.
Zeng, H., Xu, W., Zang, M., Yang, P., 2020a. Calibration of DEM-FEM model parameters for traction performance analysis of an off-road tire on gravel terrain. Powder Technol. 362, 350–361.
Zeng, H., Xu, W., Zang, M., Yang, P., Guo, X., 2020b. Calibration and validation of DEM-FEM model parameters using upscaled particles based on physical experiments and simulations. Adv. Powder Technol. 31, 3947–3959.